Article

Structures and Dissolution Behaviors of Quaternary CaO-SrO-P$_2$O$_5$-TiO$_2$ Glasses

Sungho Lee [1,2,*], Fukue Nagata [1], Katsuya Kato [1], Takayoshi Nakano [2] and Toshihiro Kasuga [3]

1 National Institute of Advanced Industrial Science and Technology (AIST), 2266-98 Anagahora, Shimoshidami, Moriyama-ku, Nagoya 463-8560, Japan; f.nagata@aist.go.jp (F.N.); katsuya-kato@aist.go.jp (K.K.)
2 Division of Materials and Manufacturing Science, Graduate School of Engineering, Osaka University, 2-1 Yamadaoka, Suita, Osaka 565-0871, Japan; nakano@mat.eng.osaka-u.ac.jp
3 Division of Advanced Ceramics, Graduate School of Engineering, Nagoya Institute of Technology, Gokiso-cho, Showa-ku, Nagoya 466-8555, Japan; kasuga.toshihiro@nitech.ac.jp
* Correspondence: sungho.lee@aist.go.jp; Tel.: +81-52-736-7711

Abstract: Calcium phosphate glasses have a high potential for use as biomaterials because their composition is similar to that of the mineral phase of bone. Phosphate glasses can dissolve completely in aqueous solution and can contain various elements owing to their acidity. Thus, the glass can be a candidate for therapeutic ion carriers. Recently, we focused on the effect of strontium ions for bone formation, which exhibited dual effects of stimulating bone formation and inhibiting bone resorption. However, large amounts of strontium ions may induce a cytotoxic effect, and there is a need to control their releasing amount. This work reports fundamental data for designing quaternary CaO-SrO-P$_2$O$_5$-TiO$_2$ glasses with pyro- and meta-phosphate compositions to control strontium ion-releasing behavior. The glasses were prepared by substituting CaO by SrO using the melt-quenching method. The SrO/CaO mixed composition exhibited a mixed cation effect on the glassification degree and ion-releasing behavior, which showed non-linear properties with mixed cation compositions of the glasses. Sr^{2+} ions have smaller field strength than Ca^{2+} ions, and the glass network structure may be weakened by the substitution of CaO by SrO. However, glassification degree and chemical durability of pyro- and meta-phosphate glasses increased with substituted all CaO by SrO. This is because titanium groups in the glasses are closely related to their glass network structure by SrO substitution. The P-O-Ti bonds in pyrophosphate glass series and TiO$_4$ tetrahedra in metaphosphate glass series increased with substitution by SrO. The titanium groups in the glasses were crosslink and/or coordinate phosphate groups to improve glassification degree and chemical durability. Sr^{2+} ion releasing amount of pyrophosphate glasses with >83% SrO substitution was larger than 0.1 mM at day seven, an amount that reported enhanced bone formation by stimulation of osteogenic markers.

Keywords: bioactive glass; phosphate glass; structure; dissolution behavior; strontium

1. Introduction

Therapeutic inorganic ions such as silicate, phosphate, magnesium, calcium, and strontium ions have been reported to stimulate tissue regeneration [1,2]. Silicate ions have been reported to improve the proliferation and differentiation of osteoblasts by stimulating insulin-like growth factor II (IGF-II) [3], alkaline phosphatase (ALP), and osteocalcin [4]. Phosphate ions are the main components of bones and stimulate the expression of matrix Gla protein to improve bone formation [5]. Magnesium ions enhance osteoblast adhesion, proliferation, differentiation, and calcification [6]. Calcium ions upregulate the expression of IGF-I and IGF-II [7] and stimulate the formation of extracellular matrix for calcification [8]. Strontium ions have two main effects: the stimulation of osteoblast proliferation and differentiation and the inhibition of preosteoclast differentiation [9–11]. The ions contribute to an improvement in cell proliferation by upregulating c-fos and egr-1, promoting

osteoblast metabolism by activating calcium-sensing receptors, and stimulating ALP and osteopontin, which are markers for osteoblast differentiation [7,11–14]. In addition, strontium ions downregulate receptor activators of nuclear factor kappa B (RANK) ligand expression, which relates to the differentiation of pre-osteoblasts by upregulation of osteoprotegerin (OPG; known as an osteoclastogenesis inhibitory factor) [10]. The strontium-substituted hydroxyapatite scaffolds with an 0.05 of Sr/(Ca + Sr) molar ratio enhanced cell proliferation, ALP activity, calcification, and OPG. By contrast, the scaffold with the ratio of 0.1 showed cytotoxic effect on mouse osteoblastic cells (MC3T3-E1) [15]. Moghanian et al. reported that 58S bioactive glasses containing 5 mol% SrO exhibited stimulation of proliferation and ALP activity on MC3T3-E1 cells, whereas the glass containing 10 mol% SrO exhibited cytotoxic effect on the cells [16]. Strontium-containing 45S5 bioglasses were upregulated osteogenic markers in vitro, such as bone morphogenetic protein-2, osteopontin, bone sialoprotein, and osteocalcin, and enhanced bone formation in vivo [17]. Accordingly, strontium ions for biomedical applications may need to control their amount without cytotoxicity.

Calcium phosphate glasses have high potential for use as biomaterials because their composition is similar to that of the mineral phase of bone. Phosphate glasses can dissolve completely in an aqueous solution [18,19] and can contain more elements than silicate glass owing to their acidity [20]. Accordingly, the glass can be a candidate for a therapeutic ion carrier. However, phosphate glass has comparably high solubility and may induce inhibition of cell growth [21]. Thus, the solubility of phosphate glasses must be controlled for biomedical applications. Titanium dioxide is known to improve the chemical durability of phosphate glasses because Ti^{4+} ions improve the cross-linking of phosphate groups [22,23]. $CaO-P_2O_5-TiO_2$ invert glass (denoted by PIG) has been the focus of research in our group [24,25]. PIG is composed of short phosphate groups, such as ortho- ($Q_P{}^0$) and pyrophosphates ($Q_P{}^1$) [24]. Titanium dioxide in PIG forms P-O-Ti bonds, resulting in enhanced glass-forming ability and chemical durability [25]. In our previous works, we demonstrated that phosphate invert glasses contained various therapeutic ions, such as Mg^{2+} [26–28], Sr^{2+} [29,30], Zn^{2+} [31], Ag^+ [32] and Nb^{5+} [33,34] ions, and controlled their release behavior. Zinc- and niobium-containing phosphate invert glasses exhibit high chemical durability because these ions improve the cross-linking of phosphate groups [25,31]. In the case of magnesium-containing phosphate invert glasses, Mg^{2+} ions formed P-O-Mg bonds and crosslinked phosphate groups. However, the bonds were easily hydrolyzed in aqueous solutions; accordingly, magnesium-containing phosphate invert glasses had smaller chemical durability [35]. Strontium ions in phosphate invert glasses decrease chemical durability owing to their smaller field strength [29]. The ion-releasing behaviors of the phosphate invert glasses are strongly related to the glass network structure. Thus, investigating the glass structure is necessary to control ion-releasing behavior, which can improve the therapeutic activity of phosphate glasses.

The present work represents a fundamental study of strontium ions for designing novel bioactive phosphate glasses with controlled release of therapeutic ions. Strontium ions have dual effects on osteoblasts and osteoclasts and are used for bone fracture in patients with osteoporosis [36,37]. In our previous work, $Na_2O-CaO-SrO-P_2O_5-TiO_2$ and $MgO-CaO-SrO-P_2O_5-TiO_2$ quinary invert glasses reported an ion-releasing amount of approximately 6% at day 7 [29,30]. Recently, our group focused on radio frequency magnetron sputtering (RF-sputtering) for the preparation of coating layer using phosphate invert glass target [38]. The coating layer exhibited comparably larger chemical durability, and the dissolution rate was 10 nm/day. However, metaphosphate groups were found in the coating layer, where the groups were not existed in the target glass. The metaphosphate groups in the coating layer may induce decreasing chemical durability, since metaphosphate groups easily hydrolyze compared to short phosphate groups [39], such as pyro- and orthophosphate. Thus, the target glass may need to improve chemical durability, using a RF-sputtering method. In this work, we prepared $CaO-SrO-P_2O_5-TiO_2$ quaternary glasses with pyro- and meta-phosphate compositions, where Na_2O and MgO in quinary glass systems were substituted by TiO_2 for further improvement of chemical durability. The

structures and ion-releasing behaviors of CaO-SrO-P_2O_5-TiO_2 quaternary glasses were evaluated.

2. Materials and Methods

2.1. Preparation of CaO-SrO-P_2O_5-TiO_2 Glasses

Two phosphate glass series were prepared wherein CaO was substituted by SrO with nominal compositions of $(60-a)$CaO·aSrO·30P_2O_5·10TiO_2 (mol%, denoted by PIG-xSr) and $(45-b)$CaO·bSrO·50P_2O_5·5TiO_2 (mol%, denoted by MPG-ySr), as listed in Table 1. Calcium carbonate ($CaCO_3$), strontium carbonate ($SrCO_3$), phosphoric acid (H_3PO_4, liquid), and titanium oxide (TiO_2) were used for preparing the batch mixtures, and all reagents were purchased from Kishida Chemical Co., Osaka, Japan. The reagents were mixed in distilled water to produce a slurry, and the mixtures were dried at 140 °C overnight. The resulting products for the PIG-xSr and MPG-ySr series were melted in a platinum crucible at 1500 and 1400 °C, respectively, for 30 min. The melts were poured onto a stainless-steel plate and pressed with another stainless-steel plate for quenching. The crystalline and opaque parts were removed manually, and optically clear PIG-xSr and MPG-ySr were obtained.

Table 1. Nominal compositions in mol% of the glasses and glass code.

Glass Code	CaO	SrO	P_2O_5	TiO_2	SrO for CaO Substitution (%)
Phosphate invert glass series					
PIG-0Sr	60	-	30	10	0
PIG-17Sr	50	10	30	10	16.7
PIG-33Sr	40	20	30	10	33.3
PIG-50Sr	30	30	30	10	50.0
PIG-67Sr	20	40	30	10	66.7
PIG-83Sr	10	50	30	10	83.3
PIG-100Sr	-	60	30	10	100
Metaphosphate glass series					
MPG-0Sr	45	-	50	5	0
MPG-25Sr	33.75	11.25	50	5	25
MPG-50Sr	22.5	22.5	50	5	50
MPG-75Sr	11.25	33.75	50	5	75
MPG-100Sr	-	45	50	5	100

2.2. Characterization of CaO-SrO-P_2O_5-TiO_2 Glass Structures

The densities of PIG-xSr and MPG-ySr were measured by an Archimedes method with glass pieces of 500–1000 mg using water as an immersion fluid. Oxygen density, which is the index of the compactness of the glass network, was calculated using the following equation [40,41]:

$$\rho_{oxygen} = \frac{M_O \times \{[CaO] + [SrO] + 5[P_2O_5] + 2[TiO_2]\}}{M_{glass}/\rho_{glass}} \tag{1}$$

where M_O is the atomic weight of oxygen, M_{glass} is the molar weight of PIG-xSr or MPG-ySr. $[CaO]$, $[SrO]$, $[P_2O_5]$, and $[TiO_2]$ are the molar fractions of calcium oxide, strontium oxide, phosphate, and titanium dioxide, respectively, and ρ_{glass} is the experimental density of PIG-xSr or MPG-ySr.

The glass structures of PIG-xSr and MPG-ySr were evaluated using laser Raman spectroscopy in the region of Raman shifts between 550 and 1400 cm^{-1} (NRS-2000, JASCO Co., Tokyo, Japan). The glasses were excited at 514.5 nm by an Ar laser with a power of 20 mW and exposure time of 30 s with an accumulation number of 16. The obtained Raman spectra of PIG-xSr and MPG-ySr were deconvoluted by assuming Gaussian spectral lines for quantitative analysis using a multipeak fitting package (Igor Pro 8, WaveMetrics Inc., Portland, OR, USA).

2.3. Thermal Analysis of CaO-SrO-P₂O₅-TiO₂ Glasses

The thermal properties of PIG-*x*Sr and MPG-*y*Sr were evaluated using differential thermal analysis (DTA, Thermo plus TG8120, 5 K/min, Rigaku Co., Tokyo, Japan). The glass transition (T_g) and onset of crystallization (T_c) temperatures of PIG-*x*Sr and MPG-*y*Sr were obtained from the DTA traces. The glassification degree (*GD*) was calculated using the following equation [42,43]:

$$GD = \frac{T_c - T_g}{T_c} \left[\frac{K}{K} \right] \qquad (2)$$

and it was used as an index of ability for glass-forming ability.

2.4. Dissolution Behavior of CaO-SrO-P₂O₅-TiO₂ Glasses

PIG-*x*Sr and MPG-*y*Sr were pulverized and sieved to a particle size of 125–250 μm to investigate their ion-releasing behavior. A 50 mM Tris-HCl solution (TBS) was prepared by dissolving tris(hydroxymethyl)aminomethane ($NH_2C(CH_2OH)_3$, Kishida Chemical Co., Osaka, Japan) in distilled water and adjusting the pH to 7.4 with 1M HCl at 37 °C. Fifteen milligrams of the glass powder was soaked in 15 mL of TBS for 7 days at 37 °C. The concentrations of Ca^{2+}, Sr^{2+}, phosphate, and Ti^{4+} ions in the TBS were measured using inductively coupled plasma-atomic emission spectroscopy (ICP-AES, ICPS-7000, Shimadzu Co., Kyoto, Japan). The molar releasing fraction of each ion was calculated using the following equation [44,45]:

$$Release\ precentage\ (\%) = \frac{\left(\frac{C_{ion}}{M_{w.atom}} \right) \times 10^5}{\left(\frac{Frac_{mol} \times M_{w.glass}}{m_{glass} \times V_{solution}} \right)} \qquad (3)$$

where C_{ion} (mg/L) is the concentration of the ion of interest, $M_{w.atom}$ (g) is the atomic weight of the respective element, $Frac_{mol}$ is the nominal molar fraction of the ions in the glass, $M_{w.glass}$ (g) is the molar weight of the glass, m_{glass} (g) is the mass of the soaked glass powder, and $V_{solution}$ (L) is the volume of TBS.

3. Results

Figure 1 shows the density and oxygen density of PIG-*x*Sr and MPG-*y*Sr. The densities of PIG-*x*Sr and MPG-*y*Sr increased from 3.00 to 3.69 and from 2.67 to 3.16 g·cm⁻³, respectively, with increase in SrO substitution percentage. The oxygen densities of PIG-*x*Sr and MPG-*y*Sr decreased from 1.31 to 1.20 and from 1.30 to 1.27 g·cm⁻³, respectively, with an increase in SrO substitution percentage.
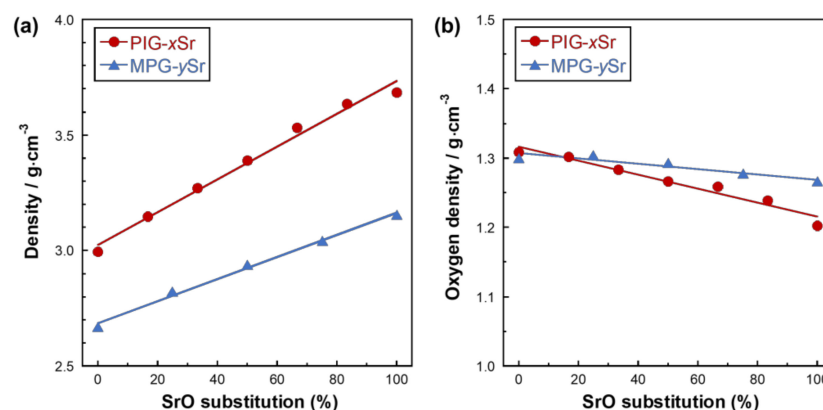

Figure 1. (**a**) Densities and (**b**) calculated oxygen densities of PIG-*x*Sr (circle) and (**b**) MPG-*y*Sr (triangle) as a function of SrO substitution percentage.

The Raman spectra and the band and peak assignments of PIG-xSr and MPG-ySr are presented in Figure 2 and Table 2, respectively. PIG-xSr exhibited Raman bands corresponding to the phosphate Q_P^0 and Q_P^1 groups [35,46,47], TiO$_4$ tetrahedra, and TiO$_6$ octahedra [24,48]. MPG-ySr exhibited Raman bands corresponding to the phosphate Q_P^1 and Q_P^2 groups [35,46,49,50] and TiO$_4$ tetrahedra [24,48].
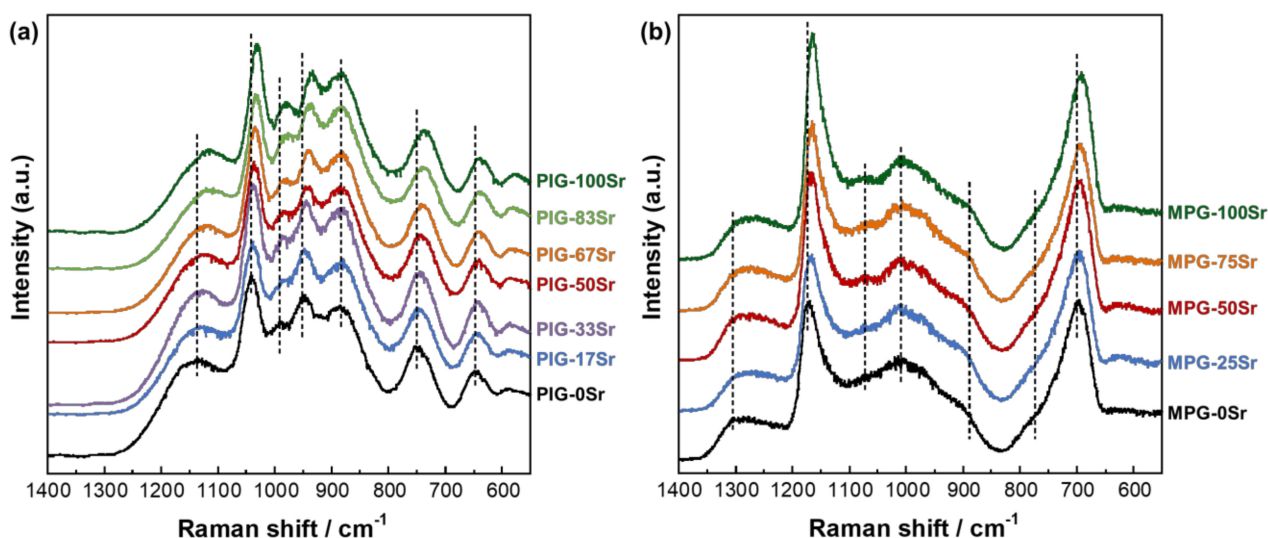

Figure 2. Laser Raman spectra for (**a**) PIG-xSr and (**b**) MPG-ySr.

Table 2. Raman band assignments for PIG-xSr and MPG-ySr.

Raman Shift/cm^{-1}	Assignments
585	P-O symmetric stretching vibration mode of Q_P^0
640	Ti-O stretching vibration mode of TiO$_6$ octahedra
695	POP symmetric stretching mode of bridging oxygen (Q_P^2 long chain)
740	POP symmetric stretching mode of bridging oxygen (Q_P^2 short chain)
745, 770	POP symmetric stretching mode of bridging oxygen (Q_P^1)
890	Ti-O stretching vibration mode of TiO$_4$ tetrahedra
945	PO$_4$ symmetric stretching mode of non-bridging oxygen (Q_P^0)
990	P-O-Ti bonds
1005, 1035	PO$_3$ symmetric stretching mode of non-bridging oxygen (Q_P^1)
1095	P-O vibration mode of the terminal for phosphate chains
1125	P-O stretching mode of the terminal Q_P^1
1150	PO$_2$ symmetric stretching mode of non-bridging oxygen (Q_P^2 long chain)
1170	PO$_2$ symmetric stretching mode of non-bridging oxygen (Q_P^2 short chain)
1265	PO$_2$ asymmetric stretching mode of non-bridging oxygen (Q_P^2)

The Raman spectra of PIG-xSr and MPG-ySr were simulated by assuming Gaussian lines for quantitative analysis. In the case of MPG-ySr, the Raman band corresponding to the POP symmetric stretching mode of bridging oxygen (700 cm^{-1}) was deconvoluted as Q_P^2 long/short chains and Q_P^1 [51], and the band corresponding to the PO$_2$ symmetric stretching mode of non-bridging oxygen (1170 cm^{-1}) was deconvoluted into Q_P^2 long and short chains [51]. The peaks of the phosphate groups in PIG-xSr were red-shifted on increasing the SrO substitution percentage. The TiO$_6$ octahedra and P-O-Ti bonds were red-shifted, whereas the positions of TiO$_4$ were not significantly different from that after

SrO substitution. The peaks of the phosphate and TiO$_4$ groups in MPG-ySr were also red-shifted when the SrO substitution percentage increased.

The integrated peak intensities of the deconvoluted bands were normalized by the sum of $I(\text{TiO}_6) + I(\text{POP}_{\text{sym}}) + I(\text{TiO}_4) + I((\text{PO}_4)_{\text{sym}}) + I(\text{P-O-Ti}) + I((\text{PO}_3)_{\text{sym}}) + I(\text{P-O}_{\text{term}}(Q_P^1))$ and $I(\text{POP}_{\text{sym\_long}}(Q_P^2)) + I(\text{POP}_{\text{sym\_short}}(Q_P^2)) + I(\text{POP}_{\text{sym}}(Q_P^1)) + I(\text{TiO}_4) + I((\text{PO}_3)_{\text{sym}}) + I(\text{P-O}_{\text{term}}(Q_P^1 \text{ or } Q_P^2)) + I((\text{PO}_2)_{\text{sym\_long}}) + I((\text{PO}_2)_{\text{sym\_short}}) + I((\text{PO}_2)_{\text{asym}})$ for PIG-xSr and MPG-ySr, respectively, where I denotes the amplitude of each peak. The normalized integrated intensities of the glasses are shown as a function of SrO substitution percentage in Figure 3. The integrated intensity of Q_P^0 and P-O$_{\text{term}}(Q_P^1)$ groups in PIG-xSr decreased, whereas that of POP$_{\text{sym}}$ and (PO$_3$)$_{\text{sym}}$ groups increased with an increase in SrO substitution percentage. Furthermore, the integrated intensity of TiO$_4$ tetrahedra and P-O-Ti bonds increased with an increase in SrO substitution percentage, whereas that of TiO$_6$ octahedra showed no significant difference. In the case of MPG-ySr, the intensity of POP$_{\text{sym\_long}}$ (Q_P^2) and (PO$_3$)$_{\text{sym}}$ decreased, whereas that of (PO$_2$)$_{\text{sym}}$, P-O$_{\text{term}}$ (Q_P^1 or Q_P^2), and TiO$_4$ tetrahedra increased with an increase in SrO substitution percentage. The intensity of POP$_{\text{sym\_short}}$ (Q_P^2), (PO$_2$)$_{\text{asym}}$, and POP$_{\text{sym}}$ (Q_P^1) showed no significant difference or a slight decreasing tendency.
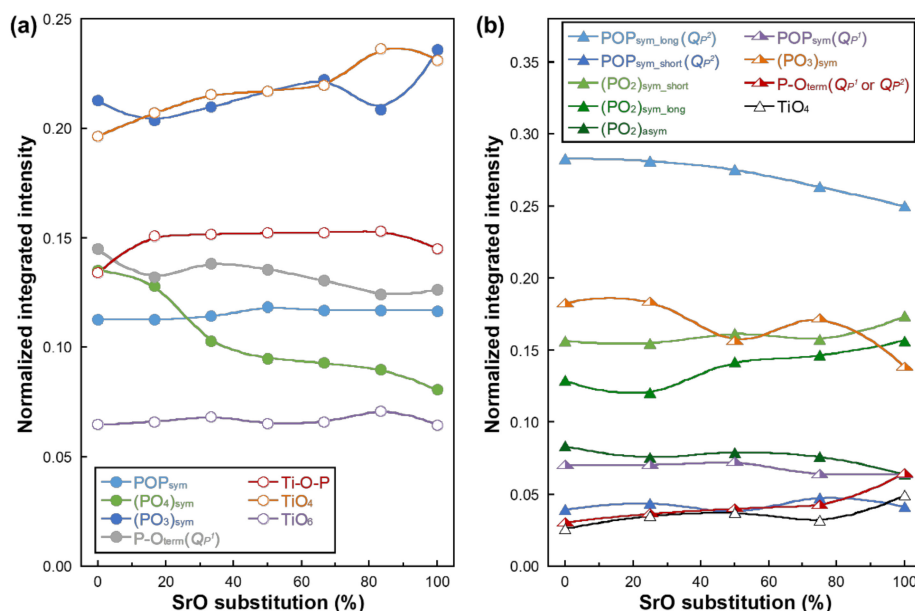

Figure 3. Normalized integrated peak intensities of (**a**) PIG-xSr (circle) and (**b**) MPG-ySr (triangle) as a function of SrO substitution percentage.

Figure 4 shows the T_g, T_c, and GD of PIG-xSr and MPG-ySr. The T_g values of PIG-xSr formed a U-shaped curve between 642 and 665 °C, with the value of PIG-33Sr as the minimum and that of PIG-100Sr as the maximum. The T_c values of PIG-xSr showed no significant difference or only a slight increase; the values varied from 706 to 719 °C. The GDs of PIG-xSr varied n-shaped curve between 0.056 and 0.074, with that of PIG-67Sr as the maximum and that of PIG-100Sr as the minimum. T_g and T_c values of MPG-ySr showed a decreasing tendency from 577 to 533 °C and from 710 to 663 °C, respectively. The GDs of MPG-ySr varied n-shaped curve between 0.183 and 0.151, with that of MPG-50Sr as the maximum and that of MPG-0Sr as the minimum.
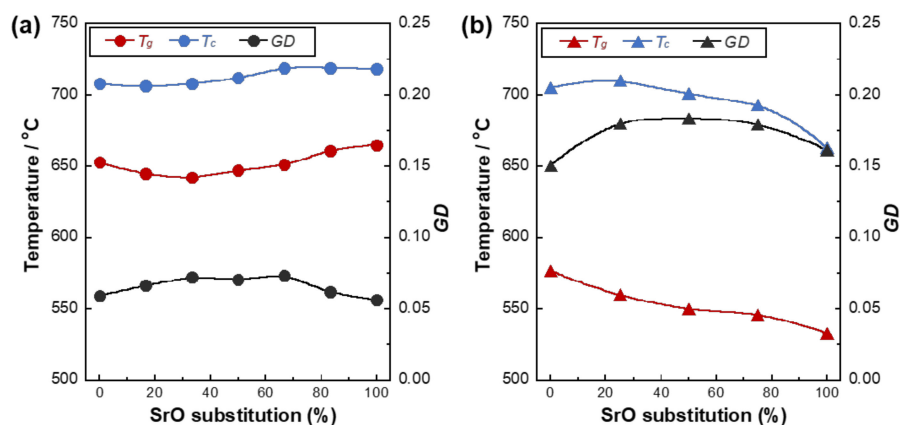
Figure 4. T_g, T_c and *GD* for (**a**) PIG-*x*Sr (circle) and (**b**) MPG-*y*Sr (triangle).

Figures 5 and 6 show the ion-releasing percentages of PIG-*x*Sr and MPG-*y*Sr, respectively, into TBS, relative to the original amount in the glasses. The releasing profiles of Ca^{2+} and Sr^{2+} ions were plotted individually and considering their sum ($Ca^{2+} + Sr^{2+}$). The ion-releasing percentages of PIG-*x*Sr resulted in U-shaped curves with an increase in SrO substitution percentage. The ion-releasing percentage of PIG-100Sr was slightly smaller than that of PIG-0Sr, and that of PIG-50Sr was the lowest. The percentages of Ca^{2+}, Sr^{2+}, ($Ca^{2+} + Sr^{2+}$), phosphate, and Ti^{4+} ions at day 7 varied between 2.4% and 3.9%, 2.2% and 3.2%, 2.3% and 3.9%, 2.6% and 4.0%, and 2.3% to 3.9%, respectively. The ion-releasing behavior of MPG-*y*Sr exhibited a non-linear decreasing tendency with an increase in SrO substitution percentage. The ion-releasing percentages decreased from MPG-0Sr to MPG-50Sr and had no significant difference between MPG-50Sr, MPG-75Sr, and MPG-100Sr. The values of Ca^{2+}, Sr^{2+}, ($Ca^{2+} + Sr^{2+}$), phosphate, and Ti^{4+} ions at day 7 decreased from 6.0% to 2.2%, 2.5% to 1.7%, 6.0% to 1.8%, 4.6% to 1.6%, and 5.3% to 1.6%, respectively.
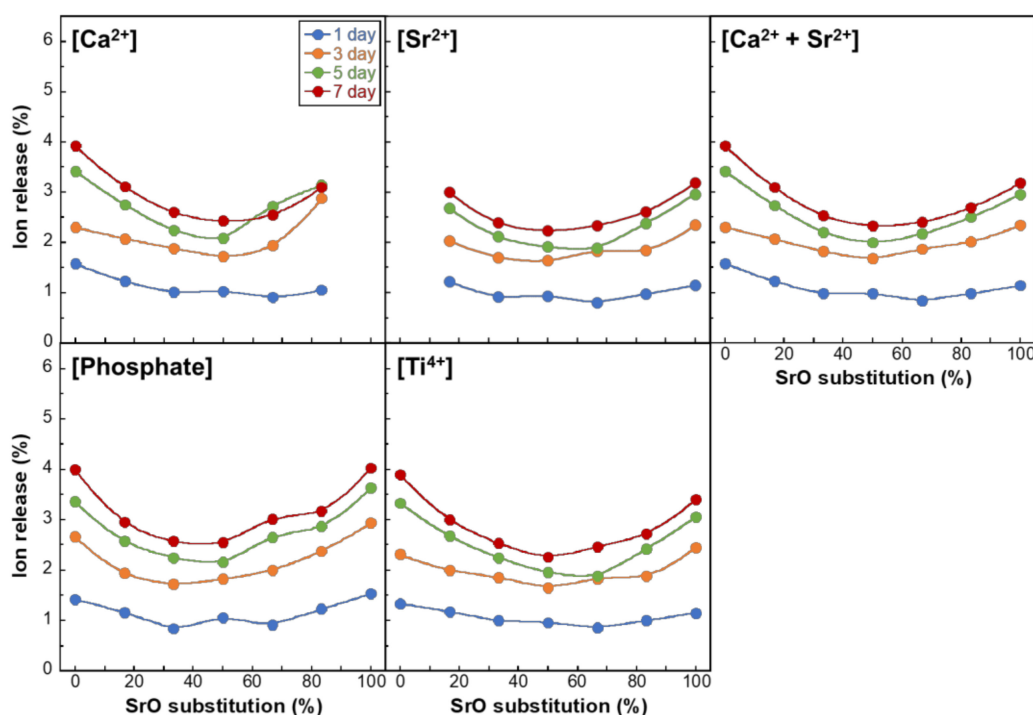

Figure 5. Percentage of ions release into TBS relative to the total amounts in PIG-*x*Sr for Ca^{2+}, Sr^{2+}, $Ca^{2+} + Sr^{2+}$, phosphate, and Ti^{4+} ions as a function of SrO substitution percentage.
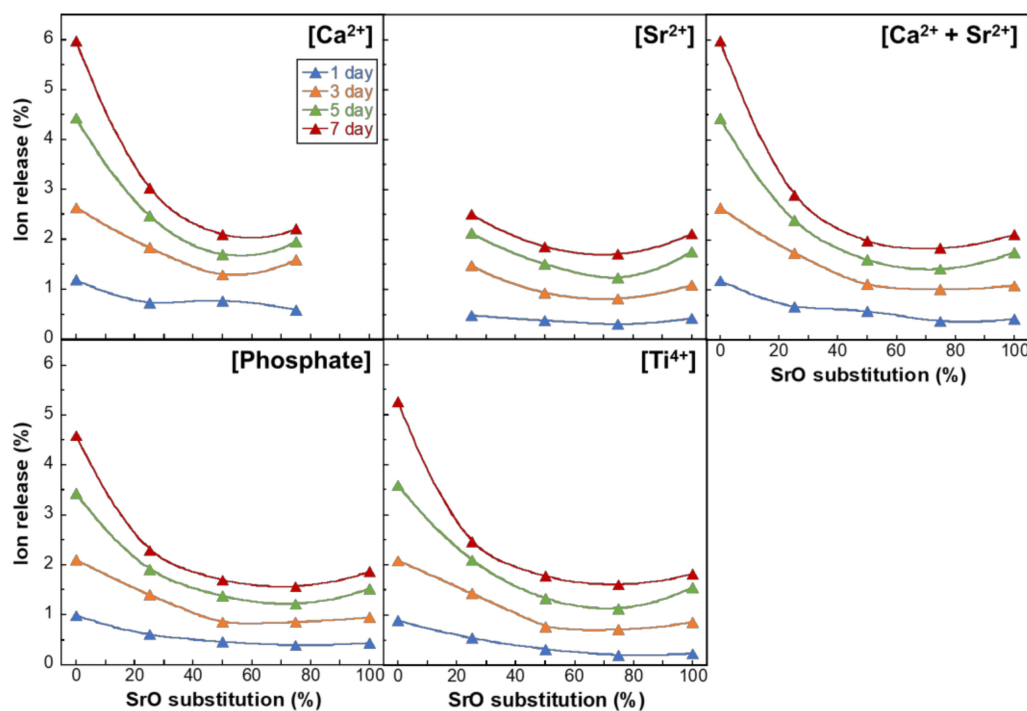
Figure 6. Percentage of ions release into TBS relative to the total amounts in MPG-*y*Sr for Ca^{2+}, Sr^{2+}, $Ca^{2+} + Sr^{2+}$, phosphate, and Ti^{4+} ions as a function of SrO substitution percentage.

4. Discussion

The density of PIG-*x*Sr and MPG-*y*Sr increased with an increase in SrO substitution percentage because the atomic weight of Sr (87.62) is larger than that of Ca (40.08), and the corresponding molar weight of the glass also increased with SrO substitution. However, the oxygen density of PIG-*x*Sr and MPG-*y*Sr decreased with an increase in SrO substitution percentage. The oxygen density, which is an index of the compactness of the glass network structure [40,41], of PIG-*x*Sr and MPG-*y*Sr, decreased with an increase in SrO substitution percentage. The ionic radii of Sr^{2+} (0.127 nm) is larger than that of Ca^{2+} ions (0.106 nm), and the corresponding ionic distances between oxygen ion are 0.248 and 0.269 nm, respectively [52]. Thus, the larger Sr^{2+} ions expanded the glass network, and the oxygen density of PIG-*x*Sr and MPG-*y*Sr decreased with the substitution of CaO by SrO. The rate of change in density and oxygen density of PIG-*x*Sr was larger than that of MPG-*y*Sr. PIG-*x*Sr is classified as 'invert glass' which contains a larger amount of network modifiers than network formers in their composition [53], whereas phosphate groups are composed of short phosphate chains, such as $Q_P{}^0$ and $Q_P{}^1$ [24]. Invert glasses did not have a continuous random network, such as a chain structure, and consisted of glass-forming tetrahedra and modifier ions linked through their non-bridging oxygen (NBO) [53]. Thus, the influence of SrO substitution on the glass network structure of PIG-*x*Sr was more than that on the structure of MPG-*y*Sr. Consequently, PIG-*x*Sr exhibited higher changing rates of density and oxygen density than MPG-*y*Sr.

The phosphate group peaks of PIG-*x*Sr and MPG-*y*Sr were red-shifted when the SrO substitution percentage increased. The bonding strength between the cation and oxygen in the glass network structure may be explained roughly by the field strength (*F*), given by the following equation [52]:

$$F = \frac{Z_c}{d^2} \left(valance/\text{Å}^2 \right) \tag{4}$$

where Z_c is the valence of the cation and d is the interatomic distance between the cation and oxygen ions. The field strength of strontium and calcium are 0.28 and 0.33 valence/Å^2, respectively. Accordingly, the bonding strength of Sr-O is weaker than that of Ca-O.

Phosphate glasses are composed of phosphate groups and cations as network formers and modifiers, respectively. The cations, i.e., Ca^{2+} and Sr^{2+} ions, in PIG-xSr and MPG-ySr are coordinated with phosphate groups to form the glass network structure. Raman peaks of phosphate groups in phosphate glasses were red-shifted on increasing the atomic number of alkaline earth metals [54] owing to a decrease in the bonding strength between phosphate and cations [55]. Thus, the peaks of the phosphate groups in PIG-xSr and MPG-ySr were red-shifted on increasing the SrO substitution percentage owing to the weaker bonding strength of Sr^{2+} compared to that of Ca^{2+} ions. Similarly, the peaks of TiO_6 octahedra and P-O-Ti bonds in PIG-xSr and TiO_4 tetrahedra in MPG-ySr exhibited a red-shift with an increase in SrO substitution percentage. In contrast, the peaks of TiO_4 tetrahedra in PIG-xSr showed no significant difference. The Raman peak positions were associated species of cations around the target groups [54], as discussed previously. Hence, the network structure around the TiO_4 tetrahedra in PIG-xSr did not change with SrO substitution.

The integrated intensities of Q_P^0 ($(PO_4)_{sym}$) and terminal Q_P^1 decreased, whereas those of Q_P^1 (POP_{sym}, $(PO_3)_{sym}$), TiO_4 tetrahedra, and P-O-Ti bonds increased with increasing SrO substitution percentage in PIG-xSr. The component rate in the glass can be assumed with integrated intensities of the Raman peaks [25]. Thus, phosphate groups in PIG-xSr exhibited decreasing and increasing tendencies for Q_P^0 and Q_P^1, respectively. However, the terminal Q_P^1 group (P-O_{term}) exhibited a decreasing tendency. This may be caused by Ti-O groups in PIG-xSr. In our previous work, TiO_4 tetrahedra acted as a network former and formed P-O-Ti bonds in phosphate invert glasses [25,56]. In addition, terminal Q_P^1 groups preferentially bond with TiO_4 tetrahedra in phosphate invert glasses [56,57]. The peak of TiO_4 tetrahedra in PIG-xSr exhibited no shift with SrO substitution. This indicates that the TiO_4 tetrahedra coordinated and/or bonded preferentially to the Q_P^1 group, regardless of the SrO content in the glass. Accordingly, P-O-Ti bonds in PIG-xSr increased by the bond between the terminal Q_P^1 group and TiO_4 tetrahedra. Accordingly, the integrated intensity of P-O_{term} exhibited a decreasing tendency with increasing SrO substitution percentage. The representative structural change in PIG-xSr with SrO substitution is an increasing component of Q_P^1 and P-O-Ti bonds.

Raman peaks of Q_P^2 groups corresponding to POP and $(PO_2)_{sym}$ in MPG-ySr were deconvoluted with long and short chains [51]. The long chain of Q_P^2 groups decreased with increasing SrO substitution percentage, whereas the short chain exhibited an opposite trend. Thus, the phosphate chains (Q_P^2 group) in MPG-ySr were broken from long to short chains. Accordingly, the NBO and terminal Q_P^2 group exhibited an increasing tendency with SrO substitution. Strontium and calcium in metaphosphate glasses exhibit coordination numbers of 7.8 and 6.6, respectively, based on the results of structural simulation [58]. These cations are coordinated with NBO in the phosphate group, and strontium requires more NBO than calcium in the glass network structure. Thus, the shortening of the Q_P^2 chain length may have originated from the larger coordination number of strontium in metaphosphate glasses. The TiO_4 tetrahedra group in MPG-ySr increased with SrO substitution. TiO_4 tetrahedra have been reported to act as a network former in phosphate glasses [25,59,60]. Thus, phosphate groups in MPG-ySr were strongly crosslinked and/or coordinated by TiO_4 tetrahedra groups. The POP_{sym} group in Q_P^1 of MPG-ySr exhibited little change with SrO substitution, and NBO in Q_P^1 decreased. This was caused by the increased TiO_4 tetrahedra groups in MPG-ySr after SrO substitution; the group may be coordinated preferentially with NBO in the Q_P^1 group. The representative structural change in MPG-ySr with SrO substitution is the shortening of the Q_P^2 chain length and crosslinking and/or coordinating of phosphate groups with TiO_4 tetrahedra.

T_g and T_c are the temperatures at which the molecules begin to move and crystallize, respectively, and these temperatures are related to the glass network structure. The T_g and T_c values of PIG-0Sr were smaller values than those of PIG-100Sr. Q_P^1 groups and P-O-Ti bonds increased with SrO substitution in PIG-xSr, as discussed previously. Hence, the glass network structure of PIG-100Sr was more crosslinked with P-O-Ti bonds, as its T_g and T_c values were larger than those of PIG-0Sr. MPG-ySr exhibited opposite trends compared

with PIG-xSr, where the T_g and T_c values of MPG-0Sr were larger than those of MPG-100Sr. The Q_P^2 group of MPG-ySr was transformed from a long chain to a short chain by SrO substitution, as mentioned above. Thus, the smaller T_g and T_c values of MPG-100Sr are related to the comparably short Q_P^2 chain structure of the glass, which may require less energy for the movement and crystallization of the molecules.

The *GD*s of PIG-100Sr and MPG-100Sr are expected to have smaller values than those of PIG-0Sr and MPG-0Sr as Sr^{2+} ions exhibit smaller field strength than Ca^{2+} ions, i.e., the bonding of the Sr^{2+} ion strength is smaller. However, the *GD*s of PIG-100Sr and PIG-0Sr exhibited similar values, whereas that of MPG-100Sr was larger than that of MPG-0Sr. This was owing to the corresponding glass network structures. The amount of P-O-Ti bonds in PIG-100Sr is larger than that in PIG-0Sr, and the bond is expected to improve *GD* owing to the crosslinking of phosphate groups. Substituted Sr^{2+} ion induced a decrease in *GD* of PIG-xSr, because phosphate glasses with a short phosphate chain, i.e., invert glasses, formed their network structure via interactions between modifier ions and phosphate groups [61]. Consequently, the *GD* of PIG-100Sr was similar to that of PIG-0Sr because the value presumably increased as the P-O-Ti bonds increased and decreased as the SrO substitution percentage increased. The phosphate chain group of MPG-100Sr was coordinated with TiO_4 tetrahedra, which can act as a network former. As a result, the *GD* of MPG-100Sr was larger than that of MPG-0Sr. The *GD*s of PIG-xSr and MPG-ySr were approximately 0.06 and 0.16, respectively. Ouchetto et al. reported that *GD*s of metaphosphate glasses and invert glasses were approximately 0.20 and 0.07, respectively [42]. Additionally, *GD*s of our previous phosphate invert glasses were 0.05~0.08 [25,27,29,30]. Thus, the *GD*s of PIG-xSr and MPG-ySr were in good agreement with previous reports of invert and metaphosphate glasses, respectively.

T_g and *GD* for PIG-xSr and T_c and *GD* for MPG-ySr exhibited non-linear trends as a function of SrO substitution percentage. PIG-xSr and MPG-ySr were prepared by the substitution of CaO by SrO. Mixed cation glasses exhibited non-linear trends in their properties [41,62,63], and these trends were also observed in our previous studies on mixed cation glasses [26,29,35]. PIG-xSr and MPG-ySr may indicate a mixed cation effect. This effect is associated with the movement of the cation in the glass network structure [64,65]. Smaller ions strongly reduce their mobility by weakly polarized oxygens that belong to larger ions [64]. In mixed cation glass, the cations in the glass network structure are located at energetically favorable sites [65], and the ions block each other's pathway for migration [66]; As a result, the ions require energy for their movement. Thus, non-linear trends in the thermal properties of PIG-xSr and MPG-ySr were believed to be due to the mixed cation effect; similar trends were observed in our previous work on phosphate glasses with the substitution of CaO with MgO [35].

All of the ions, such as [Ca^{2+} + Sr^{2+}], phosphate, Ti^{4+} ions, in the glasses released at similar rates. Thus, the glasses showed congruent dissolution, which indicated that no selective ion leaching occurred, similar to our previous phosphate glasses [25]. The field strength of Sr^{2+} ions is smaller than that of Ca^{2+} ions, and the bonding strength of cations in the glass network structure is expected to decrease with SrO substitution. As a result, the substitution of SrO with CaO may decrease the chemical durability of glasses. However, the ion-releasing percentages of PIG-100Sr and MPG-100Sr were smaller than those of PIG-0Sr and MPG-0Sr, respectively. PIG-xSr and MPG-ySr contain TiO_2 in their composition, and the components are reported to improve the chemical durability of phosphate glasses [23,67]. Additionally, the P-O-Ti bonds in the PIG-xSr and TiO_4 tetrahedra in MPG-ySr increased with SrO substitution. Thus, the structural changes of titanate groups in PIG-xSr and MPG-ySr with SrO substitution improved the chemical durability by crosslinking and/or coordinating with the phosphate groups. The SrO/CaO mixed compositions of PIG-xSr and MPG-ySr exhibited non-linear trends in ion-releasing behavior, which may indicate the mixed cation effect. The glasses with mixed cation compositions exhibited larger chemical durability than single cation glasses [62,63]. In our previous works on phosphate glasses, the chemical durability of mixed cation compositions

was larger than that of single cation compositions [29,30,35]. In PIG-*x*Sr and MPG-*y*Sr, the chemical durability improved by structural changes in the titanium group, and SrO/CaO-mixed compositions exhibited the mixed cation effect on ion-releasing behavior. Barbara et al. reported that 0.1~1 mM of Sr^{2+} ion exhibited stimulation of ALP activity and collagen synthesis in MC3T3-E1 cells [12]. In our previous MgO-CaO-SrO-P_2O_5-TiO_2 invert glasses exhibited stimulation of ALP activity in MC3T3-E1 cells, where the glasses indicated Sr^{2+} ion releasing amount of above 0.1 mM at day 7 [30]. Sr^{2+} ion releasing amount of PIG-83Sr and -100Sr was larger than 0.1 mM at day 7, whereas the amount of MPG-100Sr was 0.04 mM. Thus, PIG-83Sr and -100Sr would be expected to enhance bone formation by stimulation of ALP activity.

5. Conclusions

The structure and dissolution behaviors of quaternary CaO-SrO-P_2O_5-TiO_2 glasses with pyro- and meta-phosphate compositions and CaO substituted by SrO were investigated. The substitution of CaO by SrO may weaken the glass network structure in PIG-*x*Sr and MPG-*y*Sr glasses because the field strength of Sr^{2+} ions is lower than that of Ca^{2+} ions. However, *GD* and chemical durability of PIG-100Sr and MPG-100Sr were improved compared with those of PIG-0Sr and MPG-0Sr, respectively. The titanium groups in PIG-*x*Sr and MPG-*y*Sr were closely related to their glass network structures by SrO substitution. Furthermore, the P-O-Ti bonds in PIG-*x*Sr and TiO_4 tetrahedra in MPG-*y*Sr increased with substitution by SrO. These structural changes induced improvements in *GD* and chemical durability of PIG-100Sr and MPG-100Sr. The SrO/CaO-mixed compositions of PIG-*x*Sr and MPG-*y*Sr exhibited the mixed cation effect on *GD* and ion-releasing behavior, which showed non-linear trends as a function of SrO substitution percentage. These glasses may be suitable candidates for controlled Sr^{2+}, Ca^{2+}, and phosphate ion-releasing biomaterials on efficient design of their glass network structures.

Author Contributions: Conceptualization, S.L., F.N., K.K., T.N. and T.K.; methodology, S.L. and T.K.; validation, S.L. and T.K.; formal analysis, S.L.; investigation, S.L. and T.K.; resources, S.L. and T.K.; data curation, S.L. and T.K.; writing—original draft preparation, S.L.; writing—review and editing, S.L., F.N., K.K., T.N. and T.K.; visualization, S.L.; supervision, T.K.; project administration, S.L., T.N. and T.K.; funding acquisition, S.L., T.N. and T.K. All authors have read and agreed to the published version of the manuscript.

Institutional Review Board Statement: Not applicable.

Informed Consent Statement: Not applicable.

Data Availability Statement: Data sharing is not applicable to this article.

Conflicts of Interest: The authors declare no conflict of interest.

References

1. Hoppe, A.; Güldal, N.S.; Boccaccini, A.R. A review of the biological response to ionic dissolution products from bioactive glasses and glass-ceramics. *Biomaterials* **2011**, *32*, 2757–2774. [CrossRef]
2. Hoppe, A.; Mourino, V.; Boccaccini, A.R. Therapeutic inorganic ions in bioactive glasses to enhance bone formation and beyond. *Biomater. Sci.* **2013**, *1*, 254–256. [CrossRef] [PubMed]
3. Xynos, I.D.; Edgar, A.J.; Buttery, L.D.K.; Hench, L.L.; Polak, J.M. Ionic products of bioactive glass dissolution increase proliferation of human osteoblasts and induce insulin-like growth factor II mRNA expression and protein synthesis. *Biochem. Biophys. Res. Commun.* **2000**, *276*, 461–465. [CrossRef]
4. Xynos, I.D.; Hukkanen, J.M.V.; Batten, J.J.; Buttery, D.L.; Hench, L.L.; Polak, M.J. Bioglass®45S5 stimulates osteoblast turnover and enhances bone formation in vitro: Implications and applications for bone tissue engineering. *Calcif. Tissue Int.* **2000**, *67*, 321–329. [CrossRef]
5. Julien, M.; Khoshniat, S.; Lacreusette, A.; Gatius, M.; Bozec, A.; Wagner, E.F.; Wittrant, Y.; Masson, M.; Weiss, P.; Beck, L.; et al. Phosphate-dependent regulation of MGP in osteoblasts: Role of ERK1/2 and Fra-1. *J. Bone Miner. Res.* **2009**, *24*, 1856–1868. [CrossRef]

6.　Yamada, S.; Ota, Y.; Obata, A.; Kasuga, T. Osteoblast-like cell responses to ion products released from magnesium- and silicate-containing calcium carbonates. *Bio Med. Mater. Eng.* **2017**, *28*, 47–56. [CrossRef]

7.　Marie, P.J. The calcium-sensing receptor in bone cells: A potential therapeutic target in osteoporosis. *Bone* **2010**, *46*, 571–576. [CrossRef] [PubMed]

8.　Maeno, S.; Niki, Y.; Matsumoto, H.; Morioka, H.; Yatabe, T.; Funayama, A.; Toyama, Y.; Taguchi, T.; Tanaka, J. The effect of calcium ion concentration on osteoblast viability, proliferation and differentiation in monolayer and 3D culture. *Biomaterials* **2005**, *26*, 4847–4855. [CrossRef] [PubMed]

9.　Marie, P.J. Strontium ranelate: A physiological approach for optimizing bone formation and resorption. *Bone* **2006**, *38*, 10–14. [CrossRef]

10.　Marie, P.J. Strontium ranelate: New insights into its dual mode of action. *Bone* **2007**, *40*, S5–S8. [CrossRef]

11.　Chattopadhyay, N.; Quinn, S.J.; Kifor, O.; Ye, C.; Brown, E.M. The calcium-sensing receptor (CaR) is involved in strontium ranelate-induced osteoblast proliferation. *Biochem. Pharmacol.* **2007**, *74*, 438–447. [CrossRef]

12.　Barbara, A.; Delannoy, P.; Denis, B.G.; Marie, P.J. Normal matrix mineralization induced by strontium ranelate in MC3T3-E1 osteogenic cells. *Metabolism* **2004**, *53*, 532–537. [CrossRef]

13.　Xue, W.; Moore, J.L.; Hosick, H.L.; Bose, S.; Bandyopadhyay, A.; Lu, W.W.; Cheung, K.M.C.; Luk, K.D.K. Osteoprecursor cell response to strontium-containing hydroxyapatite ceramics. *J. Biomed. Mater. Res. A* **2006**, *79*, 804–814. [CrossRef] [PubMed]

14.　Qiu, K.; Zhao, X.J.; Wan, C.X.; Zhao, C.S.; Chen, Y.W. Effect of strontium ions on the growth of ROS17/2.8 cells on porous calcium polyphosphate scaffolds. *Biomaterials* **2006**, *27*, 1277–1286. [CrossRef] [PubMed]

15.　Kim, H.-W.; Kim, Y.-J. Fabrication of strontium-substituted hydroxyapatite scaffolds using 3D printing for enhanced bone regeneration. *J. Mater. Sci.* **2021**, *56*, 1673–1684. [CrossRef]

16.　Moghanian, A.; Firoozi, S.; Tahriri, M.; Sedghi, A. A comparative study on the in vitro formation of hydroxyapatite, cytotoxicity and antibacterial activity of 58S bioactive glass substituted by Li and Sr. *Mater. Sci. Eng. C* **2018**, *91*, 349–360. [CrossRef]

17.　Zhang, X.; Cui, J.; Cheng, L.; Lin, K. Enhancement of osteoporotic bone regeneration by strontium-substituted 45S5 bioglass via time-dependent modulation of autophagy and the Akt/mTOR signaling pathway. *J. Mater. Chem. B* **2021**. [CrossRef]

18.　Knowles, J.C. Phosphate based glasses for biomedical applications. *J. Mater. Chem.* **2003**, *13*, 2395–2401. [CrossRef]

19.　Brauer, D.S. Phosphate Glasses. *Bio Glasses* **2012**, 45–64. [CrossRef]

20.　Kasuga, T. Glass-based biomaterials design for generating advanced functions. *J. Jpn. Soc. Biomater.* **2016**, *34*, 66–70.

21.　Abou Neel, E.A.; Pickup, D.M.; Valappil, S.P.; Newport, R.J.; Knowles, J.C. Bioactive functional materials: A perspective on phosphate-based glasses. *J. Mater. Chem.* **2009**, *19*, 690–701. [CrossRef]

22.　Brow, R.K.; Tallant, D.R.; Warren, W.L.; McIntyre, A.; Day, D.E. Spectroscopic studies of the structure of titanophosphate and calcium titanophosphate glasses. *Phys. Chem. Glasses* **1997**, *38*, 300–306.

23.　Brauer, D.S.; Karpukhina, N.; Law, R.V.; Hill, R.G. Effect of TiO2 addition on structure, solubility and crystallisation of phosphate invert glasses for biomedical applications. *J. Non Cryst. Solids* **2010**, *356*, 2626–2633. [CrossRef]

24.　Kasuga, T.; Abe, Y. Calcium phosphate invert glasses with soda and titania. *J. Non Cryst. Solids* **1999**, *243*, 70–74. [CrossRef]

25.　Lee, S.; Maeda, H.; Obata, A.; Ueda, K.; Narushima, T.; Kasuga, T. Structures and dissolution behaviors of $CaO–P_2O_5–TiO_2/Nb_2O_5$ ($Ca/P \geq 1$) invert glasses. *J. Non Cryst. Solids* **2015**, *426*, 35–42. [CrossRef]

26.　Morikawa, H.; Lee, S.; Kasuga, T.; Brauer, D.S. Effects of magnesium for calcium substitution in $P_2O_5–CaO–TiO_2$ glasses. *J. Non Cryst. Solids* **2013**, *380*, 53–59. [CrossRef]

27.　Lee, S.; Maeda, H.; Obata, A.; Ueda, K.; Narushima, T.; Kasuga, T. Structure and dissolution behavior of $MgO-P_2O_5-TiO_2/Nb_2O_5$ ($Mg/P \geq 1$) invert glasses. *J. Ceram. Soc. Jpn.* **2015**, *123*, 942–948. [CrossRef]

28.　Lee, S.; Nagata, F.; Kato, K.; Kasuga, T. Dissolution behavior of $MgO-CaO-P_2O_5-TiO_2$ invert glasses. *Phosphorus Res. Bull.* **2020**, *36*, 10–14. [CrossRef]

29.　Lee, S.; Obata, A.; Kasuga, T. Ion release from $SrO-CaO-TiO_2-P_2O_5$ glasses in Tris buffer solution. *J. Ceram. Soc. Jpn.* **2009**, *117*, 935–938. [CrossRef]

30.　Lee, S.; Obata, A.; Brauer, D.S.; Kasuga, T. Dissolution behavior and cell compatibility of alkali-free $MgO-CaO-SrO-TiO_2-P_2O_5$ glasses for biomedical applications. *Biomed. Glasses* **2015**, *1*, 151–158. [CrossRef]

31.　Lee, S.; Uehara, H.; Maçon, A.L.B.; Maeda, H.; Obata, A.; Ueda, K.; Narushima, T.; Kasuga, T. Preparation of antibacterial $ZnO-CaO-P_2O_5-Nb_2O_5$ invert glasses. *Mater. Trans.* **2016**, *57*, 2072–2076. [CrossRef]

32.　Lee, S.; Nakano, T.; Kasuga, T. Structure, dissolution behavior, cytocompatibility, and antibacterial activity of silver-containing calcium phosphate invert glasses. *J. Biomed. Mater. Res. A* **2017**, *105*, 3127–3135. [CrossRef]

33.　Obata, A.; Takahashi, Y.; Miyajima, T.; Ueda, K.; Narushima, T.; Kasuga, T. Effects of niobium ions released from calcium phosphate invert glasses containing Nb_2O_5 on osteoblast-like cell functions. *Acs Appl. Mater. Interfaces* **2012**, *4*, 5684–5690. [CrossRef] [PubMed]

34.　Maeda, H.; Lee, S.; Miyajima, T.; Obata, A.; Ueda, K.; Narushima, T.; Kasuga, T. Structure and physicochemical properties of $CaO–P_2O_5–Nb_2O_5–Na_2O$ glasses. *J. Non Cryst. Solids* **2016**, *432*, 60–64. [CrossRef]

35.　Lee, S.; Maeda, H.; Obata, A.; Ueda, K.; Narushima, T.; Kasuga, T. Structures and dissolution behaviors of $MgO–CaO–P_2O_5–Nb_2O_5$ glasses. *J. Non Cryst. Solids* **2016**, *438*, 18–25. [CrossRef]

36. Meunier, P.J.; Roux, C.; Seeman, E.; Ortolani, S.; Badurski, J.E.; Spector, T.D.; Cannata, J.; Balogh, A.; Lemmel, E.-M.; Pors-Nielsen, S.; et al. The effects of strontium ranelate on the risk of vertebral fracture in women with postmenopausal osteoporosis. *N. Engl. J. Med.* **2004**, *350*, 459–468. [CrossRef] [PubMed]

37. Pors Nielsen, S. The biological role of strontium. *Bone* **2004**, *35*, 583–588. [CrossRef]

38. Sato, P.S.; Watanabe, T.; Maeda, H.; Obata, A.; Kasuga, T. Preparation of an antibacterial amorphous thin film by radiofrequency magnetron sputtering using a 65ZnO–30P$_2$O$_5$–5Nb$_2$O$_5$ glass. *J. Non Cryst. Solids* **2020**, *528*, 119724. [CrossRef]

39. Bunker, B.C.; Arnold, G.W.; Wilder, J.A. Phosphate glass dissolution in aqueous solutions. *J. Non Cryst. Solids* **1984**, *64*, 291–316. [CrossRef]

40. Ray, N.H. Composition—property relationships in inorganic oxide glasses. *J. Non Cryst. Solids* **1974**, *15*, 423–434. [CrossRef]

41. Tylkowski, M.; Brauer, D.S. Mixed alkali effects in Bioglass® 45S5. *J. Non Cryst. Solids* **2013**, *376*, 175–181. [CrossRef]

42. Ouchetto, M.; Elouadi, B.; Parke, S. Study of lanthanide zinc phosphate glasses by differential thermal analysis. *Phys. Chem. Glasses* **1991**, *32*, 22–28.

43. Lee, S. Development of glass-related biomaterials for enhanced bone regeneration via stimulation of cell function. *J. Ceram. Soc. Jpn.* **2020**, *128*, 349–356. [CrossRef]

44. Lee, S.; Maçon, A.L.B.; Kasuga, T. Structure and dissolution behavior of orthophosphate MgO–CaO–P$_2$O$_5$–Nb$_2$O$_5$ glass and glass-ceramic. *Mater. Lett.* **2016**, *175*, 135–138. [CrossRef]

45. Lee, S.; Nakano, T.; Kasuga, T. Formation and structural analysis of 15MgO–15CaO–8P$_2$O$_5$–4SiO$_2$ glass. *J. Non Cryst. Solids* **2017**, *457*, 73–76. [CrossRef]

46. Karakassides, M.A.; Saranti, A.; Koutselas, I. Preparation and structural study of binary phosphate glasses with high calcium and/or magnesium content. *J. Non Cryst. Solids* **2004**, *347*, 69–79. [CrossRef]

47. Brow, R.K.; Tallant, D.R.; Myers, S.T.; Phifer, C.C. The short-range structure of zinc polyphosphate glass. *J. Non Cryst. Solids* **1995**, *191*, 45–55. [CrossRef]

48. Sakka, S.; Miyaji, F.; Fukumi, K. Structure of binary K2O-TiO$_2$ and Cs2O-TiO$_2$ glasses. *J. Non Cryst. Solids* **1989**, *112*, 64–68. [CrossRef]

49. Mishra, A.; Rocherullé, J.; Massera, J. Ag-doped phosphate bioactive glasses: Thermal, structural and in-vitro dissolution properties. *Biomed. Glasses* **2016**, *2*, 38–48. [CrossRef]

50. Ciceo Lucacel, R.; Hulpus, A.O.; Simon, V.; Ardelean, I. Structural characterization of phosphate glasses doped with silver. *J. Non Cryst. Solids* **2009**, *355*, 425–429. [CrossRef]

51. Le, Q.H.; Calahoo, C.; Xia, Y.; Buchheim, J.; Bragatto, C.B.; Wondraczek, L. Optimization of electrical conductivity in the Na2O-P$_2$O$_5$-AlF$_3$-SO$_3$ glass system. *J. Am. Ceram. Soc.* **2020**, *103*, 4939–4956. [CrossRef]

52. Vogel, W. Classical Theories of Glass Structure. In *Glass Chemistry*; Vogel, W., Ed.; Springer: Berlin/Heidelberg, Germany, 1994; pp. 41–56.

53. Brow, R.K. Review: The structure of simple phosphate glasses. *J. Non Cryst. Solids* **2000**, *263–264*, 1–28. [CrossRef]

54. Nelson, B.N.; Exarhos, G.J. Vibrational spectroscopy of cation-site interactions in phosphate glasses. *J. Chem. Phys.* **1979**, *71*, 2739–2747. [CrossRef]

55. Rouse, G.B., Jr.; Miller, P.J.; Risen, W.M., Jr. Mixed alkali glass spectra and structure. *J. Non Cryst. Solids* **1978**, *28*, 193–207. [CrossRef]

56. Maeda, H.; Tamura, T.; Kasuga, T. Experimental and theoretical investigation of the structural role of titanium oxide in CaO-P$_2$O$_5$-TiO$_2$ invert glass. *J. Phys. Chem. B* **2017**, *121*, 5433–5438. [CrossRef] [PubMed]

57. Silva, A.M.B.; Correia, R.N.; Oliveira, J.M.M.; Fernandes, M.H.V. Structural characterization of TiO2–P$_2$O$_5$–CaO glasses by spectroscopy. *J. Eur. Ceram. Soc.* **2010**, *30*, 1253–1258. [CrossRef]

58. Christie, J.K.; de Leeuw, N.H. Effect of strontium inclusion on the bioactivity of phosphate-based glasses. *J. Mater. Sci.* **2017**, *52*, 9014–9022. [CrossRef] [PubMed]

59. Li, Y.; Weng, W.; Santos, J.D.; Lopes, A.M. Structural studies of Na$_2$O-TiO$_2$-P$_2$O$_5$ system glasses investigated by FTIR and FT-Raman. *Phys. Chem. Glasses Eur. J. Glass Sci. Technol. B* **2008**, *49*, 41–45.

60. Nagarjuna, M.; Satyanarayana, T.; Gandhi, Y.; Veeraiah, N. Influence of Ag$_2$O on some physical properties of LiF–TiO$_2$–P$_2$O$_5$ glass system. *J. Alloys Compd.* **2009**, *479*, 549–556. [CrossRef]

61. Mandlule, A.; Döhler, F.; van Wüllen, L.; Kasuga, T.; Brauer, D.S. Changes in structure and thermal properties with phosphate content of ternary calcium sodium phosphate glasses. *J. Non Cryst. Solids* **2014**, *392–393*, 31–38. [CrossRef]

62. Dilmore, M.F.; Clark, D.E.; Hench, L.L. Chemical durability of Na$_2$O-K$_2$O-CaO-SiO$_2$ glasses. *J. Am. Ceram. Soc.* **1978**, *61*, 439–443. [CrossRef]

63. Zhifang, W.; Nai, Z.; Bo, M.; Zhongxin, S. Study of the mixed alkali effect on chemical durability of alkali silicate glasses. *J. Non Cryst. Solids* **1986**, *84*, 468–476. [CrossRef]

64. Isard, J.O. The mixed alkali effect in glass. *J. Non Cryst. Solids* **1969**, *1*, 235–261. [CrossRef]

65. Day, D.E. Mixed alkali glasses—Their properties and uses. *J. Non Cryst. Solids* **1976**, *21*, 343–372. [CrossRef]

66. Swenson, J.; Adams, S. Mixed alkali effect in glasses. *Phys. Rev. Lett.* **2003**, *90*, 155507. [CrossRef] [PubMed]

67. Kishioka, A.; Haba, M.; Amagasa, M. Glass formation in multicomponent phosphate systems containing TiO$_2$. *Bull. Chem. Soc. Jpn.* **1974**, *47*, 2493–2496. [CrossRef]